DASY8/6 Modules SAR & WPT

APPLICATION NOTE

Testing Compliance with ISED SPR-002 Issue 2 (R3 05/24)

s p e a g

Testing Compliance of WPT Devices with DASY8/6 Modules SAR & WPT according to ISED SPR-002 Issue 2 (Revision 3, 05/24)

1 Scope of this Document

This application note provides guidance on how to demonstrate compliance with the basic restrictions of the local induced electric (E-) field and specific absorption rate (SAR) in accordance with Issue 2 of ISED SPR-002 [1]:

- ≥4 MHz: DASY8/6 Module SAR 16.4+ measures the induced SAR and E-fields inside the standard phantom directly and fully complies with RSS-102 [3] and ISED SPR-002 Issue 2 [1];
- <4 MHz: DASY8/6 Module WPT V2.6+ (i) measures the incident fields, including phase, in a volume equivalent to the entire half-space at high resolutions, (ii) reconstructs the Maxwell field in this volume generated by the complete WPT system that may include the transmitter and receiver, e.g., the wireless charger with the phone on top, and (iii) reconstruct the induced SAR and E-fields inside the standard phantom by means of the fully validated Sim4Life solver (P-EM-QS). The workflow does not require any modeling of the WPT system by the user. The measurement system is self-contained, i.e., it automatically verifies if all conditions for reliable and accurate evaluations are satisfied, and provides the analysis of compliance according to the latest regulations. It fully complies with RSS-102 [3] and ISED SPR-002 Issue 2 [1].

Hence, the methods described here provide the most accurate assessments of the actual maximum exposure currently available.

Note: Even though the methods are fully compatible with Sections 6 and 8 of ISED SPR-002 Issue 2 [1], submission of a statement to declare that *"The evaluation is performed according to the attached Application Note "Testing Compliance of WPT Devices with DASY8/6 Modules SAR & WPT according to ISED SPR-002 Issue 2 (Revision 3, 05/24)" issued by SPEAG whereby all requirements are met or are considered in the revised uncertainty budget ."* is recommended.

2 Summary of ISED SPR-002 Issue 2

2.1 Scope and Method

The scope of ISED SPR-002 Issue 2 [1] encompasses:

- assessments against the radiofrequency (RF) exposure limits to prevent both nerve stimulation (NS) and thermal effects
- assessments against both the reference levels (RL) and basic restrictions (BR)

- measurement-based and computational assessments

The method to assess the BR by measurements is at the top of the assessment method hierarchy (see Figure 1.1) and is, therefore, the first choice.

Note: Computational assessments based on modeling of the device-under-test (DUT) have large uncertainties, as the exposure is determined by the incident field strengths at the surface of the DUT. It is a fundamental law that the validation of the incident fields at the surface governs the uncertainty assessment of computational methods.

Note: Determination of the coverage factor usually requires hundreds of simulations with anatomical models to generate sufficient statistical power [2].

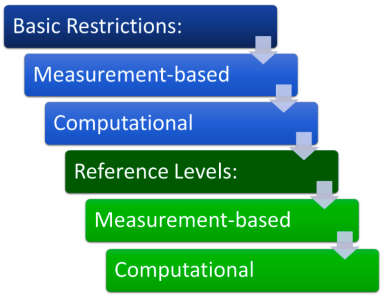

Figure 1.1: Assessment method hierarchy specified in [1]

2.2 Instrumentation Requirements

Section 5 of ISED SPR-002 Issue 2 [1] sets out the general requirements for compliance testing of wireless power transfer (WPT) devices. In particular, assessments are required to be performed at zero distance (i.e., at the touch position, especially for NS-based assessments). ISED SPR-002 Issue 2 refers to RSS-102 [3] regarding the requirements for measurement-based assessments against the BR for the SAR, whereas the requirements for measurement-based assessments against the BR for the induced E-field will be defined in a future issue.

Section 7 of ISED SPR-002 Issue 2 provides the requirements for measurement-based assessments against the RL. In particular, the detailed requirements of the probe and the sensor inside the probe are specified (Sections 7.1.6 and 7.1.7, respectively). A comparison of the specifications of the MAGPy probe Version 2 with these requirements is provided in Table 1.1. Section 8 of ISED SPR-002 Issue 2 provides the requirements for simulation-based assessments and suggests the use of the same material properties for the tissue-simulating liquid as in Section 8.3.4 of IEC/IEEE 63184 [4].

	Sensitivity [A/m or V/m]	Ampl. flatness [dB]	Linear range [A/m or V/m]	Linearity error [dB]	Sensor size[a] [mm]	Isotropy [dB]
SPR-002 Issue 2	H: $\leq$1 A/m E: $\leq$1 V/m	$\leq$1	defined as a function of RL	$\leq$0.5	$\leq d_{meas}/1.7$	$\leq$1
MAGPy probe V2	H: 0.1 A/m E: 0.08 V/m	<0.2 (typ.)	H: 0.1–3200 A/m E: 0.1–2000 V/m	H: <0.2 (typ.) E: <0.5 (typ.)	H: 10 mm E: 50 mm	<0.5 (typ.)

[a] Sensor size requirement in ISED SPR-002 Issue 2 was defined as a function of the distance relative to the center of the probe antenna, i.e., d_{meas}, in order to limit the errors in high gradient fields, i.e., integration of the sensor size

Table 1.1: Comparison of the specifications of MAGPy probe Version 2 with the probe and sensor requirements outlined in ISED SPR-002 Issue 2 [1]. **The distance requirement is not relevant for assessment with DASY8/6 Module WPT V2.6+, as the system determines the induced fields via simulations (see the note below).**

Note: The minimal distance requirements are not applied for the probe system used in DASY8/6 Module WPT V2.6+, as the system does not rely on single measurements but utilizes field reconstruction to assess the actual exposure. As the measured incident fields are the input for the simulations, validation of the DUT model is not required.

3 SPEAG's Measurement Solutions

3.1 DASY8/6 Module SAR 16.4+

DASY8/6 Module SAR 16.4+ meets all performance requirements of IEC/IEEE 62209-1528:2020 [5] and RSS-102 [3] for frequencies between 4 MHz and 10 GHz. More details about DASY8/6 Module SAR 16.4+ are provided in the DASY8/6 Module SAR 16.4+ Manual [9].

3.2 DASY8/6 Module WPT V2.6+

DASY8/6 Module WPT V2.6+ meets all performance requirements of IEC/IEEE 63814 [4]. It is composed of the isotropic probe MAGPy-8H3D+E3D Version 2, the reference probe (MAGPy-RAϕV2), and the data acquisition system (MAGPy-DAS) mounted to the DASY8/6 robot via the emergency stop (MAGPy-ES). At each probe location, 8 isotropic magnetic (H-) field values plus the phase are acquired, as well as the isotropic E-field measurement.

The field is measured on a high density grid (7.33 mm resolution) such that the incident quasi-static H-field (amplitude and phase) of the entire measured volume can be reconstructed by our advanced and validated vector potential reconstruction (see Appendix A for more information). The incident E-field distribution is measured in the same volume, enabling the accurate determination of the field impedance at $d = 30$ mm. Due to the geometric

design of the E_z-field sensor, the measured information is sufficient for a reliable estimation of the E-fields at the surface of the DUT, i.e., $d = 0$, and its potential coupling to the tissue simulating media, even for very localized E-field sources. The effect of the phantom loading or backscattering is less than 1% for frequencies <4 MHz as derived from theoretical considerations, supported by simulations and verified by measurements (see Appendix B)

The local E-field and SAR induced by the incident H-field are determined inside the standard phantom without approximation and with known uncertainty only using the measured and reconstructed fields via Sim4Life's verified Quasi-Static EM Solver (P-EM-QS) (ZMT Zurich MedTech AG). The local E-field and SAR induced by the incident E-field[1] are determined by a conservative approximation that is valid for local E-field sources [7]. The validity of the local E-field condition is automatically assessed by the system, including checking whether the field impedance is less than 10% of the plane wave impedance of 377 Ω.

The total field evaluation (see Appendix C for its validation) provides the assessed total peak local induced E-field and total peak spatial-average SAR (psSAR1g/10g), which are compared to the BR.

The dedicated graphical user interface (GUI) fully automates the testing workflow. More details about DASY8/6 Module WPT V2.6+ are provided below and in the DASY8/6 Module WPT V2.6+ Manual [6].

Note: The method implemented in DASY8/6 Module WPT V2.6+ is equivalent to the use of the validated P-EM-QS solver of Sim4Life (see Appendix D) to determine the induced E-field and SAR by simulations but without modeling the DUT and without the validation uncertainties. Thus, the method is much more accurate than compliance testing by simulations, since the only remaining uncertainty is the reconstruction and measurement uncertainty, which is typically less than 1.3 dB. For typical and realistic simulation modeling uncertainty, see [8].

4 Test System and Procedures for Frequencies ≥4 MHz

4.1 System Requirements

To determine the induced instant peak E-field ($pE_{ind,inst}$) and the peak spatial-average SAR values (psSAR1g/10g) as required by ISED SPR-002 Issue 2 [1], the following system configuration is recommended:

- DASY8/6 Module SAR software
- ELI phantom
- HBBL4-250Vx head simulating liquid
- EX3DVx probe with conversion factor assessment at 6 MHz (covers 4–9 MHz) and 13 MHz (covers 9–19 MHz)
- confined loop antennas CLA-6 and CLA-13 for system check and validation purposes

4.2 Measurement Procedure

The workflow to demonstrate compliance with the BR, illustrated in Figure 1.2, is equivalent to standard psSAR evaluations with an additional step – Determination of $pE_{ind,tissue,inst}$– described below.

[1] The highest E-field generated by WPT systems is often traceable to local charge accumulations (e.g., across the discrete capacitor to achieve resonance, at the end of conductors), which decay rapidly (proportional to $1/d^4$) but which can potentially induce strong fields in the body [7]. These charge accumulations are difficult to predict and to simulate accurately. However, this issue is overcome with DASY8/6 Module WPT V2.6+ as it uses measurements to determine the actual field characteristics and to conservatively determine the field contribution.

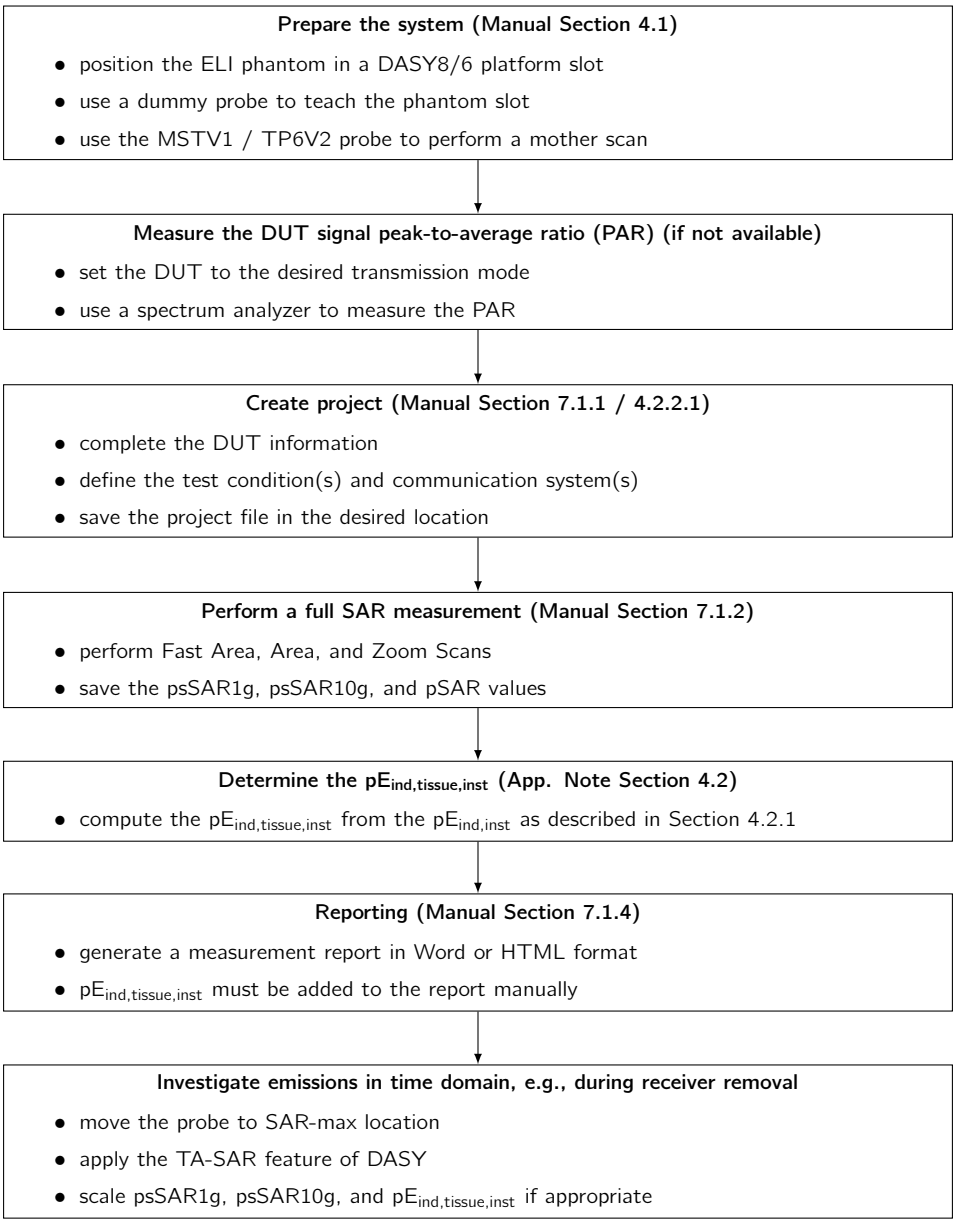

Figure 1.2: DASY8/6 Module SAR step-by-step measurement procedure

4.2.1 Determining $pE_{ind,tissue,inst}$

The psSAR1g/10g is determined from a regular Zoom Scan. In addition, DASY8/6 Module SAR 16.4+ reports the pSAR (maximum SAR at the inner phantom surface) and the $pE_{ind,inst}$ (see Figure 1.3).

Figure 1.3: $pE_{ind,tissue,inst}$ results derived from a Zoom Scan measured with DASY8/6 Module SAR 16.4+

The maximum instantaneous E-field value in non-homogeneous tissues can be calculated using Equation 1.1.

$$pE_{ind,tissue,inst} = pE_{ind,inst} \cdot CF \tag{1.1}$$

where $pE_{ind,inst}$ = maximum instantaneous E-field value at the phantom surface in V/m
CF = coverage factor, which translates the induced fields in the standardized homogeneous tissue to those in non-homogeneous tissues, after taking field enhancements at dielectric boundaries into account, as generally determined in [2]
$pE_{ind,tissue,inst}$ = maximum instantaneous E-field values in non-homogeneous tissues

Note: The 5 mm-line and 2×2×2 mm^3-cube averaged induced E-field will be directly provided in DASY8/6 Module SAR V17.0.

4.3 Uncertainty

The uncertainty for evaluation of any WPT source for psSAR1g/10g is determined according to IEC/IEEE 62209-1528:2020 [5]. Typically, the uncertainties ($k = 2$) are <22.8% for psSAR1g/10g (see Table 1.2) and <12.5% for $pE_{ind,inst}$, based on the assumption of a maximum extrapolation uncertainty of less than 5%.

DASY8/6 Uncertainty Budget
According to IEC/IEEE 62209-1528
(Frequency band: 4 MHz–300 MHz range)

Symbol	Error Description	Unc. Value	Prob. Dist.	Div.	(c_i) (1 g)	(c_i) (10 g)	Std. Unc. (1 g)	Std. Unc. (10 g)
Measurement System Errors								
CF	Probe Calibration	±13.3%	N	2	1	1	±6.65%	±6.65%
CF_{drift}	Probe Calibration Drift	±1.7%	R	$\sqrt{3}$	1	1	±1.0%	±1.0%
LIN	Probe Linearity	±4.7%	R	$\sqrt{3}$	1	1	±2.7%	±2.7%
BBS	Broadband Signal	±0.6%	R	$\sqrt{3}$	1	1	±0.3%	±0.3%
ISO	Probe Isotropy	±7.6%	R	$\sqrt{3}$	1	1	±4.4%	±4.4%
DAE	Other Probe+Electronic	±0.8%	N	1	1	1	±0.8%	±0.8%
AMB	RF Ambient	±1.8%	N	1	1	1	±1.8%	±1.8%
Δ_{sys}	Probe Positioning	±0.006 mm	N	1	0.04	0.04	±0.10%	±0.10%
DAT	Data Processing	±1.2%	N	1	1	1	±1.2%	±1.2%
Phantom and Device Errors								
LIQ(σ)	Conductivity (meas.)	±2.5%	N	1	0.78	0.71	±2.0%	±1.8%
LIQ(T_σ)	Conductivity (temp.)	±5.4%	R	$\sqrt{3}$	0.78	0.71	±2.4%	±2.2%
EPS	Phantom Permittivity	±14.0%	R	$\sqrt{3}$	0	0	±0%	±0%
DIS	Distance DUT – TSL	±2.0%	N	1	2	2	±4.0%	±4.0%
D_{xyz}	Device Positioning	±1.0%	N	1	1	1	±1.0%	±1.0%
H	Device Holder	±3.6%	N	1	1	1	±3.6%	±3.6%
MOD	DUT Modulation	±2.4%	R	$\sqrt{3}$	1	1	±1.4%	±1.4%
TAS	Time-average SAR	±1.7%	R	$\sqrt{3}$	1	1	±1.0%	±1.0%
RF_{drift}	DUT drift	±2.5%	N	1	1	1	±2.5%	±2.5%
VAL	Val Antenna Unc.	±0.0%	N	1	1	1	±0%	±0%
RF_{in}	Unc. Input Power	±0.0%	N	1	1	1	±0%	±0%
Correction to the SAR results								
C(ε, σ)	Deviation to Target	±1.9%	N	1	1	0.84	±1.9%	±1.6%
C(R)	SAR scaling	±0.0%	R	$\sqrt{3}$	1	1	±0.0%	±0.0%
u(ΔSAR)	Combined Uncertainty						±11.4%	±11.3%
U	**Expanded Uncertainty**						±22.8%	±22.5%

Table 1.2: Uncertainty budget for peak 1 gram and 10 gram mass-average SAR measured with DASY8/6 Module SAR, assessed according to IEC/IEEE 62209-1528.

5 Test System and Procedures for Frequencies <4 MHz

5.1 System Requirements

To determine the induced E-field and SAR in the frequency range between 3 kHz and 4 MHz, the following equipment is required:

- DASY8/6 Module WPT V2.6+ including:
  - MAGPy-8H3D+E3D Version 2 probe (with the integrated data acquisition system MAGPy-DAS)
  - MAGy-RAϕV2 reference probe (as a phase reference)
  - MAGPy-ES emergency stop system
- WPT sources (incl. V-Coil500/3, V-Coil350/85, and V-Coil50/400) for system check and validation purposes
- Software DASY8/6 Module WPT V2.6+

5.2 Measurement Procedure

The workflow to demonstrate compliance with the BR is illustrated in Figure 1.4. Detailed descriptions of each step can be found in Section 7 of the DASY8/6 Module WPT Manual [6]. It is recommended to perform a system check before any compliance testing with the V-Coil source that operates at the frequency closest to that of the DUT. This provides the confidence that the system operates within its specifications.

5.3 Uncertainty

Guidance about the uncertainty evaluations for DASY8/6 Module WPT is provided in the Manual [6]. Typical uncertainties ($k = 2$) are <34% for psSAR1g/10g (see Tables 1.3 and 1.4) and <18% for pE_{ind} (see Table 1.5).

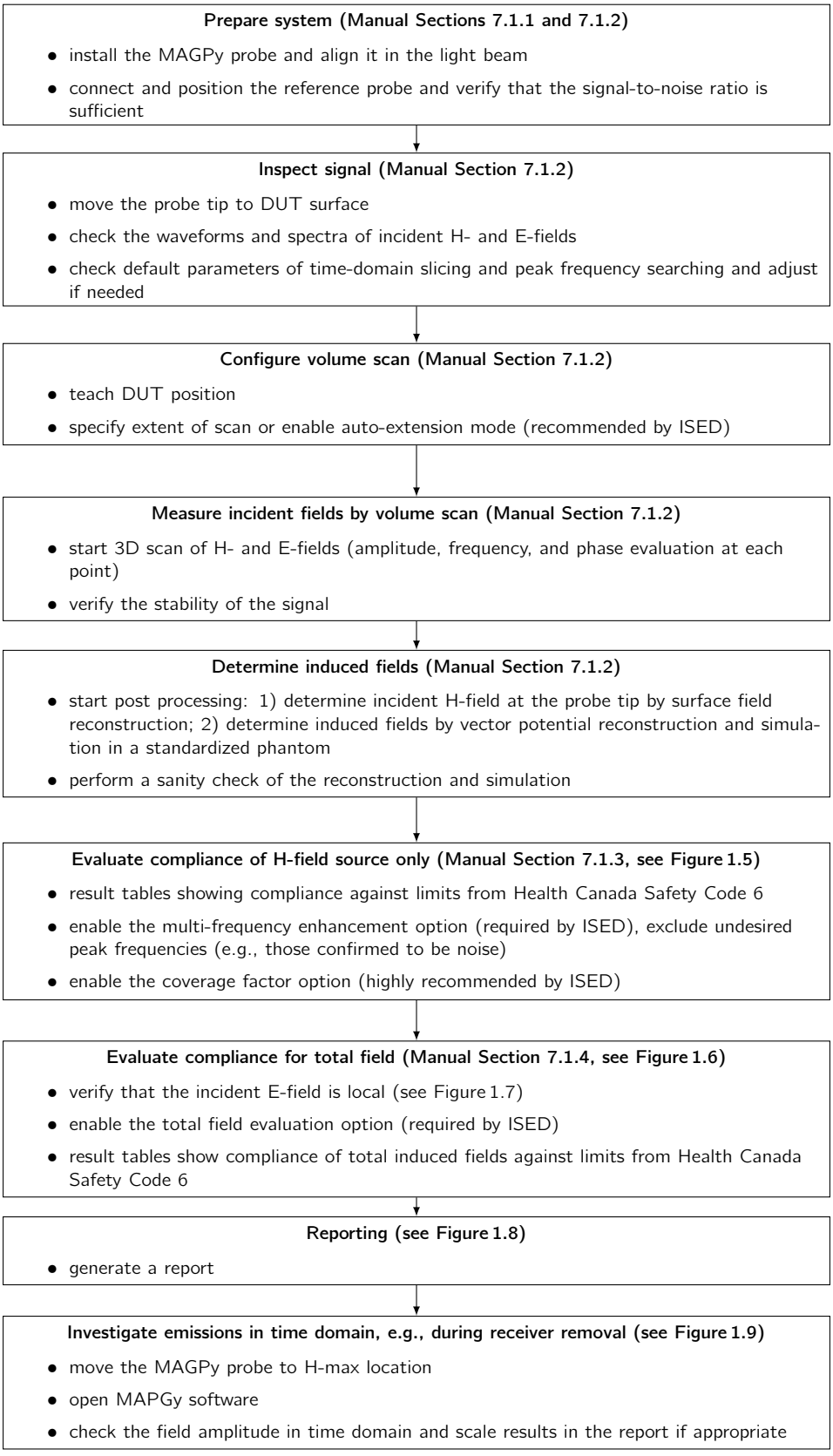

Figure 1.4: DASY8/6 Module WPT step-by-step measurement procedure

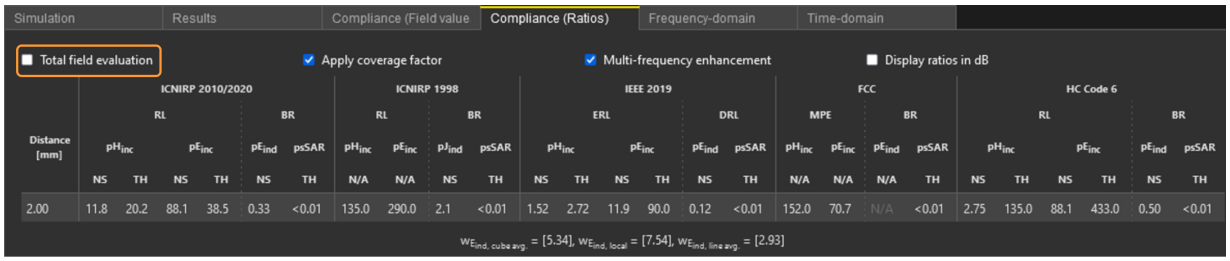

Figure 1.5: Table in the DASY8/6 Module WPT GUI showing the compliance evaluation results for the induced fields exclusively due to the incident H-field. Note that the "Total field evaluation" option (highlighted by the orange box) is un-checked in this case.

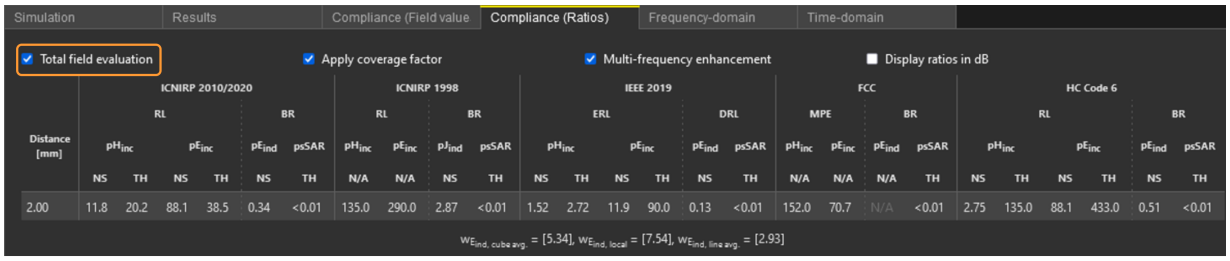

Figure 1.6: Table in the DASY8/6 Module WPT GUI showing the compliance evaluation results for the total induced fields (i.e., the exposures from both the incident H-field and E-field are assessed). Note that the "Total field evaluation" option (highlighted by the orange box) is checked in this case.

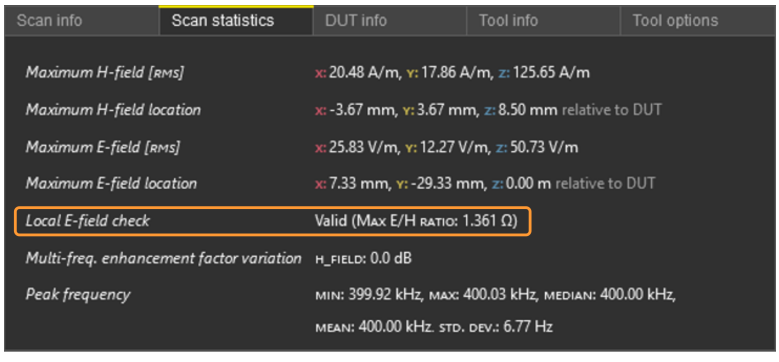

Figure 1.7: The part of the DASY8/6 Module WPT GUI for displaying the statistic information of the volume scan, e.g., the result of the local E-field check (highlighted by the orange box, where the maximum E/H ratio is also reported).

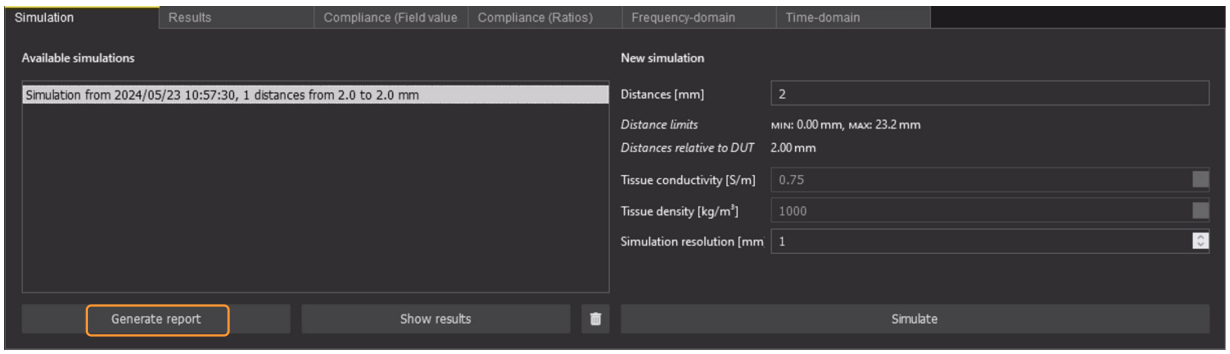

Figure 1.8: The part of the DASY8/6 Module WPT GUI for setting up the simulation and generating the report in DASY8/6 Module WPT. Note that the tissue conductivity and mass density are pre-set to standardized values and cannot be altered by users. After finishing the simulation, a report can be generated by clicking the "Generate report" button (highlighted by the orange box).

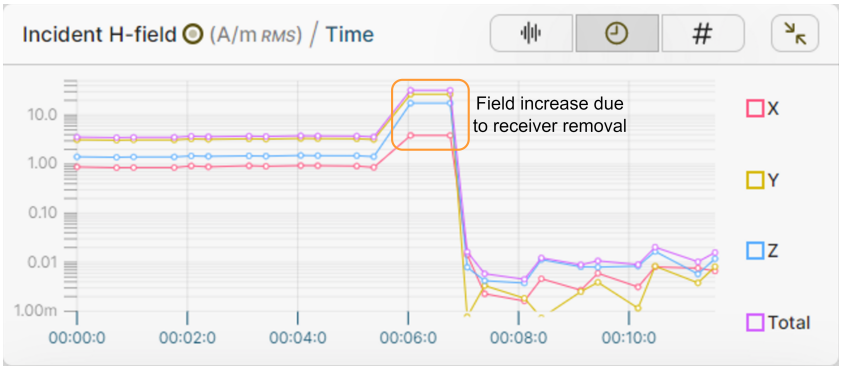

Figure 1.9: The time-domain plot of the incident H-field in the MAGPy GUI. The data were recorded from a commercial wireless charger while removing the smartphone placed on the charger. The same procedure can also be used to monitor the stability of the source.

DASY8/6 Uncertainty Budget for psSAR1g according to IEC/IEEE 63184						
Item	Error Description	Unc. Value (±dB)	Probab. Distr.	Div.	(c_i)	Std. Unc. (±dB)
Measurement system						
1	Amplitude calibration uncertainty	0.35	N	1	1	0.35
2	Probe anisotropy	0.60	R	$\sqrt{3}$	1	0.35
3	Probe dynamic linearity	0.20	R	$\sqrt{3}$	1	0.12
4	Probe frequency domain response	0.30	R	$\sqrt{3}$	1	0.17
5	Probe frequency linear interp. fit	0.15	R	$\sqrt{3}$	1	0.09
6	Spatial averaging	0.10	R	$\sqrt{3}$	1	0.06
7	Parasitic E-field sensitivity	0.10	R	$\sqrt{3}$	1	0.06
8	Detection limit	0.15	R	$\sqrt{3}$	1	0.09
9	Readout electronics	0	N	1	1	0
10	Probe positioning	0.19	N	1	1	0.19
11	Repeatability	0.10	N	1	1	0.10
12	Surface field reconstruction	0.20	N	1	1	0.20
Numerical simulations						
13	Grid resolution	0.02	R	$\sqrt{3}$	1	0.01
14	Tissue parameters	0	R	$\sqrt{3}$	1	0
15	Exposure position	0	R	$\sqrt{3}$	1	0
16	Source representation	0.09	N	1	1	0.09
17	Convergence and power budget	0	R	$\sqrt{3}$	1	0
18	Boundary conditions	0.10	R	$\sqrt{3}$	1	0.06
19	Phantom loading/backscattering	0.10	R	$\sqrt{3}$	1	0.06
Combined uncertainty ($k = 1$)						0.63
Expanded uncertainty ($k = 2$)						**1.27 (33.9%)**

Table 1.3: Uncertainty budget for peak 1 gram mass-average SAR measured with DASY8/6 Module WPT, assessed according to IEC/IEEE 63184.

DASY8/6 Uncertainty Budget for psSAR10g **according to IEC/IEEE 63184**						
Item	Error Description	Unc. Value (±dB)	Probab. Distr.	Div.	(c_i)	Std. Unc. (±dB)
Measurement system						
1	Amplitude calibration uncertainty	0.35	N	1	1	0.35
2	Probe anisotropy	0.60	R	$\sqrt{3}$	1	0.35
3	Probe dynamic linearity	0.20	R	$\sqrt{3}$	1	0.12
4	Probe frequency domain response	0.30	R	$\sqrt{3}$	1	0.17
5	Probe frequency linear interp. fit	0.15	R	$\sqrt{3}$	1	0.09
6	Spatial averaging	0.10	R	$\sqrt{3}$	1	0.06
7	Parasitic E-field sensitivity	0.10	R	$\sqrt{3}$	1	0.06
8	Detection limit	0.15	R	$\sqrt{3}$	1	0.09
9	Readout electronics	0	N	1	1	0
10	Probe positioning	0.19	N	1	1	0.19
11	Repeatability	0.10	N	1	1	0.10
12	Surface field reconstruction	0.20	N	1	1	0.20
Numerical simulations						
13	Grid resolution	0	R	$\sqrt{3}$	1	0
14	Tissue parameters	0	R	$\sqrt{3}$	1	0
15	Exposure position	0	R	$\sqrt{3}$	1	0
16	Source representation	0.04	N	1	1	0.04
17	Convergence and power budget	0	R	$\sqrt{3}$	1	0
18	Boundary conditions	0.10	R	$\sqrt{3}$	1	0.06
19	Phantom loading/backscattering	0.10	R	$\sqrt{3}$	1	0.06
Combined uncertainty ($k = 1$)						0.63
Expanded uncertainty ($k = 2$)						**1.25 (33.4%)**

Table 1.4: Uncertainty budget for peak 10 gram mass-average SAR measured with DASY8/6 Module WPT, assessed according to IEC/IEEE 63184.

DASY8/6 Uncertainty Budget for Peak Local E_{ind} according to IEC/IEEE 63184						
Item	Error Description	Unc. Value (±dB)	Probab. Distr.	Div.	(c_i)	Std. Unc. (±dB)
Measurement system						
1	Amplitude calibration uncertainty	0.35	N	1	1	0.35
2	Probe anisotropy	0.60	R	$\sqrt{3}$	1	0.35
3	Probe dynamic linearity	0.20	R	$\sqrt{3}$	1	0.12
4	Probe frequency domain response	0.30	R	$\sqrt{3}$	1	0.17
5	Probe frequency linear interp. fit	0.15	R	$\sqrt{3}$	1	0.09
6	Spatial averaging	0.10	R	$\sqrt{3}$	1	0.06
7	Parasitic E-field sensitivity	0.10	R	$\sqrt{3}$	1	0.06
8	Detection limit	0.15	R	$\sqrt{3}$	1	0.09
9	Readout electronics	0	N	1	1	0
10	Probe positioning	0.19	N	1	1	0.19
11	Repeatability	0.10	N	1	1	0.10
12	Surface field reconstruction	0.30	N	1	1	0.30
Numerical simulations						
13	Grid resolution	0.09	R	$\sqrt{3}$	1	0.05
14	Tissue parameters	0	R	$\sqrt{3}$	1	0
15	Exposure position	0	R	$\sqrt{3}$	1	0
16	Source representation	0.27	N	1	1	0.27
17	Convergence and power budget	0	R	$\sqrt{3}$	1	0
18	Boundary conditions	0.10	R	$\sqrt{3}$	1	0.06
19	Phantom loading/backscattering	0.10	R	$\sqrt{3}$	1	0.06
Combined uncertainty ($k = 1$)						0.73
Expanded uncertainty ($k = 2$)						**1.45 (18.2%)**

Table 1.5: Uncertainty budget for peak local (i.e., not spatial averaged) induced E-field measured with DASY8/6 Module WPT, assessed according to IEC/IEEE 63184.

6 Conclusions

This application note provides guidance on how to use DASY8/6 Module SAR 16.4+ and DASY8/6 Module WPT V2.6+ for measurement-based compliance testing against BR (induced E-field for nerve stimulation, SAR for thermal effect) in accordance with ISED SPR-002 Issue 2 for inductive WPT devices.

Bibliography

[1] ISED SPR-002 Issue 2, *Assessment methods of the human exposure to electric and magnetic fields from wireless power transfer systems – Models, instrumentation, measurement and computational methods and procedures (Frequency range of 3 kHz to 30 MHz)*, October 2022

[2] J. Xi, A. Christ, and N. Kuster, *Coverage factors for efficient demonstration of compliance of low-frequency magnetic near-field exposures with basic restrictions*, Physics in Medicine & Biology, vol. 68, no. 3, 2023.

[3] ISED RSS-102, *Radio frequency (RF) exposure compliance of radiocommunication apparatus (all frequency bands)*, issue 5, March 2015

[4] IEC/IEEE 63184, *Assessment methods of the human exposure to electric and magnetic fields from wireless power transfer systems – Models, instrumentation, measurement and computational methods and procedures (Frequency range of 3 kHz to 30 MHz)*, CDV, August 2023

[5] IEC/IEEE 62209-1528:2020, *Measurement procedure for the assessment of specific absorption rate of human exposure to radio frequency fields from hand-held and body-worn wireless communication devices - Part 1528: Human models, instrumentation and procedures (Frequency range of 4 MHz to 10 GHz)*, October 2020.

[6] SPEAG, *DASY8/6 Module WPT system handbook, incl. SW module WPT 2.6*, May 2024.

[7] A. Christ, A. Fallahi, E. Neufeld, Q. Balzano, and N. Kuster, *Mechanism of Capacitive Coupling of Proximal Electromagnetic Sources With Biological Bodies*, Bioelectromagnetics, vol. 43, no. 7, pp. 404–412, 2022.

[8] SPEAG Application Note, *Testing WPT devices by simulations: Guidance for best practice*, January 2024.

[9] SPEAG, *DASY8/6 Module SAR system handbook, incl. SW module SAR 16.4*, May 2024.

[10] I. Laakso, V. De Santis, S. Cruciani, T. Campi, and M. Feliziani, *Modeling of induced electric fields based on incompletely known magnetic fields*, Physics in Medicine & Biology, vol. 62, no. 16, 2017.

A Reconstruct a Vector Potential $\vec{A}$ From a Magnetic Field

The induced current simulation requires a vector potential instead of the H-field as input. The vector potential $\vec{A}$ has the property of $\mathtt{curl}(\vec{A}) = \vec{B}$, and in free space $\vec{B} = \mu_0 \vec{H}$.
This equation is non-trivial, as any additional gradient field still fulfills $\mathtt{curl}(\vec{A} + \mathtt{grad}(\phi)) = \vec{B}$. Luckily, an explicit formula, which requires $\mathtt{div}(\vec{B}) \equiv 0$ on a rectilinear grid, can be derived [10]. For the x-component, the formula reads (others are cyclic permutations)

$$A_x = -\int_0^y \left[\frac{1}{3}B_z(x,v,z) + \frac{1}{6}B_z(x,v,0)\right] \mathrm{d}v + \int_0^z \left[\frac{1}{3}B_y(x,y,w) + \frac{1}{6}B_y(x,0,w)\right] \mathrm{d}w \tag{2}$$

where the subscripts x, y, z denote the components along their corresponding axes, and v and w denote the integration variables. The axis origin, i.e., the point at which the path integrals begin to integrate, can be arbitrarily chosen. Currently, the most dominant location of the $\vec{B}$ field is chosen as the origin to minimize numerical integration artifacts. Details are provided in [10].

B Effect of Backscattering on the Source

B.1 Objectives

In this section, we assess the effect of the phantom loading or backscattering on the incident field for frequencies below 4 MHz by comparing the dissipated energy in the phantom to the H-field energy. The uncertainty in the determination of the induced fields due to the incident field without the phantom is also determined.

B.2 Theory

Maxwell's equation in the frequency domain (with linear constitutive material models) reads (see Sim4Life manual for details):

$$\nabla \times \vec{E} = -j\omega\vec{B} = -j\omega\mu\vec{H} \tag{3a}$$

$$\nabla \times \vec{H} = -j\omega\vec{D} + \vec{J} = -j\omega\epsilon\vec{E} + \sigma\vec{E} + \vec{J}_0 \tag{3b}$$

$$\nabla \times \vec{D} = \nabla \cdot \epsilon\vec{E} = \rho \tag{3c}$$

$$\nabla \times \vec{B} = \nabla \cdot \mu\vec{H} = 0 \tag{3d}$$

With a vector potential $\vec{A}$ defined as $\nabla \times \vec{A} = \vec{B} = \mu\vec{H}$ (in the Coulomb gauge, i.e., $\nabla \cdot \vec{A} = 0$), the E-field can be written as $\vec{E} = -j\omega\vec{A} - \nabla\phi$, where ϕ is an additional scalar potential. The complex permittivity $\tilde{\epsilon} := \epsilon + \frac{\sigma}{j\omega}$ and the divergence-freeness of the $\vec{A}$ allows the $\nabla \times \vec{H}$ equation to be rewritten as

$$\nabla \times \frac{1}{\mu}\nabla \times \vec{A} = \underbrace{\omega^2\tilde{\epsilon}\vec{A} - j\omega\tilde{\epsilon}\nabla\phi}_{:=\omega\text{-terms}} + \vec{J}_0 \tag{4}$$

The H-field $\vec{H}$ is the *static* H-field, i.e., it is not altered by the induced E-field, if

$$\nabla \times \frac{1}{\mu}\nabla \times \vec{A} = \vec{J}_0, \tag{5}$$

i.e., the two ω-terms are negligible. In the following, the order-of-magnitude scalings of those 2 ω-terms are investigated. The order of magnitude can be estimated by means of the in-order-of notation $\mathcal{O}(\cdot)$.

Since in a vacuum there are no free charges, i.e., ρ vanishes, the scalar and vector potential are related as $\nabla \times \epsilon\nabla\phi = -j\omega\nabla \cdot \epsilon\vec{A}$. Given a characteristic length scale L to estimate the spatial derivations, the following relationship is provided: $\mathcal{O}(\tilde{\epsilon}\phi/L^2) = \mathcal{O}(\omega\tilde{\epsilon}A/L)$, i.e, ϕ scales like $\phi = \mathcal{O}(\omega AL)$. Application of the same scaling strategy to two ω-terms in (4) yields $\mathcal{O}(\omega^2\tilde{\epsilon}A)$ in both cases. Therefore, it can be estimated

$$\frac{\texttt{both-}\omega\texttt{-terms}}{\nabla \times \frac{1}{\mu} \times A\texttt{-term}} = \mathcal{O}(\omega^2\tilde{\epsilon}\mu L^2), \tag{6}$$

i.e., written with permittivity and conductivity, the ω-terms can be neglected when

$$\omega^2\epsilon\mu L^2 \ll 1 \tag{7a}$$

$$\omega\sigma\mu L^2 \ll 1 \tag{7b}$$

Calculated values for the two ω-terms of the tissue material properties $\epsilon_r = 55$, $\sigma = 0.75\,\mathrm{S/m}$ and a reference coil diameter, where the coil diameter was used as the characteristic length, are provided in Table 6. At 4 MHz, both values are much smaller than $-20\,\mathrm{dB}$, i.e., the quasi-static conditions can still be considered as valid.

The fist criterion (7a) can be rewritten using the wave-length λ, the frequency $f = \omega/2\pi$, the speed of light within the phantom c and the relations $\sqrt{1/(\epsilon\mu)} = c = \lambda \cdot f = \lambda \cdot \omega/(2\pi)$, i.e., replacing $\omega^2\epsilon\mu$ with $(2\pi/\lambda)^2$

$$\frac{2\pi L}{\lambda} \ll 1 \quad \Longleftrightarrow \quad L \ll \frac{\lambda}{2\pi} \tag{8}$$

The second criterion in (7b) can be further simplified using the skin depth $\delta = \sqrt{2/(\omega\sigma\mu)}$ (valid if $\omega \ll \sigma/\epsilon$), i.e., replacing $\omega\sigma\mu$ with $2/\delta^2$:

$$\frac{\sqrt{2}L}{\delta} \ll 1 \quad \Longleftrightarrow \quad L \ll \frac{\delta}{\sqrt{2}} \tag{9}$$

Frequency [kHz]	Coil diameter [mm]	$\omega^2\epsilon\mu L^2$ [dB]	$\omega\sigma\mu L^2$ [dB]
3	454.0	−147.0	−48.7
85	200.0	−103.1	−33.9
400	52.5	−99.5	−43.7
1000	52.5	−83.5	−35.7
2000	52.5	−71.5	−29.7
4000	52.5	−59.5	−23.7

Table 6: Results of the calculations of the two ω-terms (i.e., $\omega^2\epsilon\mu L^2$ and $\omega\sigma\mu L^2$) for tissue material properties $\epsilon_r = 55$, $\sigma = 0.75\,\mathrm{S/m}$ and a coil diameter of 52 mm. The coil diameter was used as the characteristic length.

B.3 Simulation Evidence

As a next step, we simulate the extent of back-scattering or the loading by the phantom by comparing the energy absorbed in the phantom to the maximum stored energy in the H-field. This ratio is expressed as

$$Q^{-1} = \frac{\text{power absorpbed in the phantom}}{2\pi f(\text{maximum energy stored})} = \frac{\int_V(\rho\ \text{SAR})dV}{2\pi f W_H} \tag{10}$$

In Eqn. (10), the magnetic energy stored W_H is calculated by integrating the product of the H-field strength and the magnetic flux density over a volume that is sufficiently large for convergence, and the absorbed power in the phantom is calculated by integrating the product of the mass density and SAR over the entire volume of the phantom.

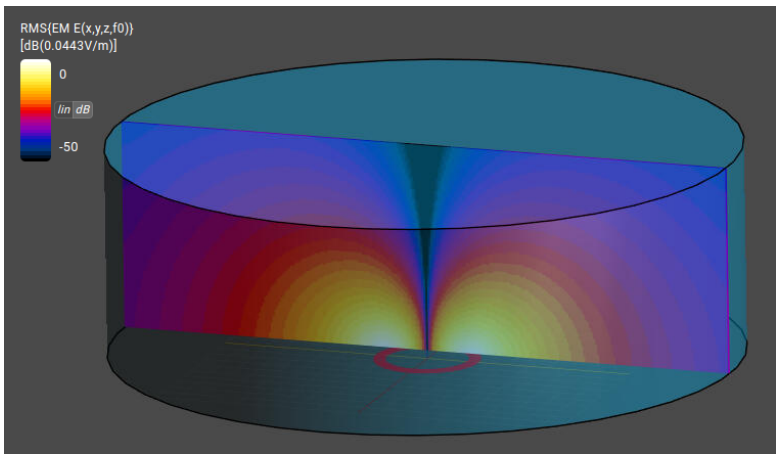

Figure 10: Normalized E-field of a generic WPT transmit coil with a diameter of 100 mm induced in a cylindrical phantom with a conductivity of 0.75 S/m placed at a distance of 4 mm.

Figure 10 shows an example of the E-field distribution in a cylindrical phantom positioned at a distance of 4 mm above a generic coil with a diameter of 100 mm simulated with the magneto quasistatic solver. According to the current draft of IEC 63184 [4], the relative permittivity of the tissue simulating liquid (TSL) in the phantom is $\epsilon_\mathrm{r} = 55$, the conductivity $\sigma = 0.75\,\mathrm{S/m}$, and the density $\rho = 1000\,\mathrm{kg/m^3}$. The effect of the phantom on the total incident H-field along the vertical center line of the coil is shown in Figure 11. The Q^{-1} values according to Eqn. (10) for the generic coil at frequencies of 400 kHz and 6.78 MHz are given in Table 7.

Frequency [kHz]	W_H [μJ]	$\int_V (\rho\ \mathrm{SAR}) dV$ [mW]	Q^{-1} [dB]
400	2.1	0.84	−30
6780	2.1	240	−18

Table 7: Maximum H-field energy and dissipated power in the phantom per $1A_{peak}$ for the 400 kHz and 6.78 kHz verification sources. The load of the phantom is <1% at frequencies <4 MHz.

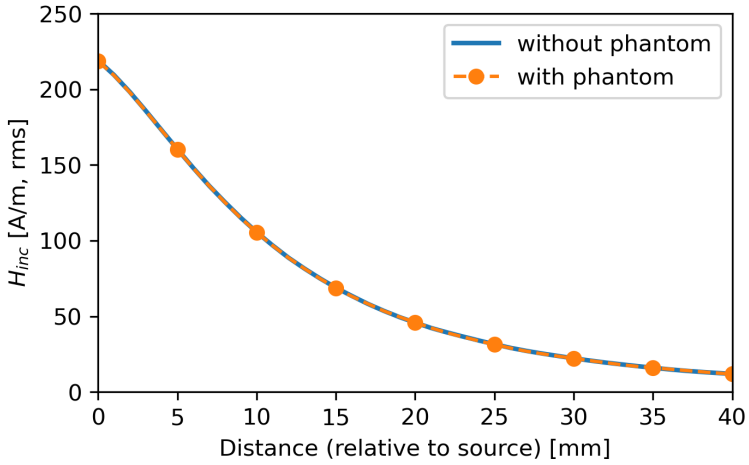

Figure 11: Comparison of the total incident H-fields (per $1A_{peak}$) along the z-axis center line of the coil with and without the phantom for the reference source V-Coil 50/400.

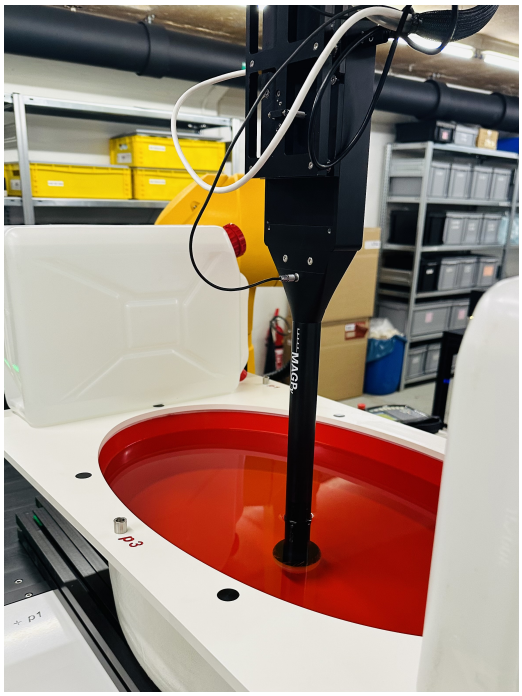

(a) Perspective view showing the probe measuring in TSL

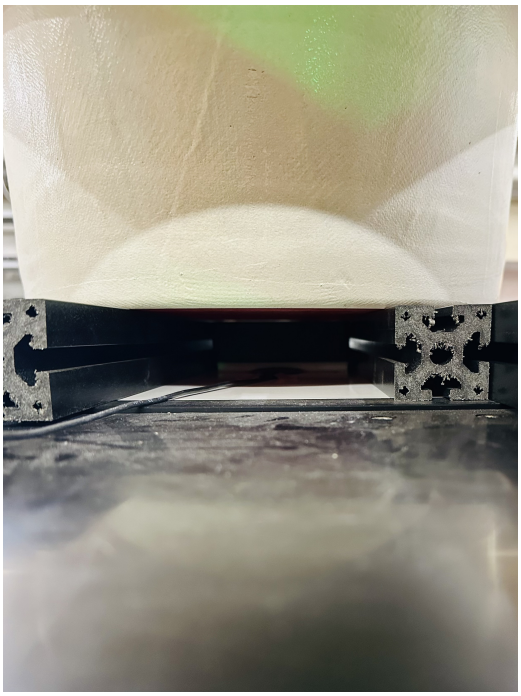

(b) Side view showing the placement of the phantom and the source

Figure 12: Setup for experimental confirmation of incident H-field insensitivity to the presence of the phantom.

B.4 Experimental Confirmation

To experimentally confirm that the effect of the phantom on the incident H-field is very small, measurements were made with a specially sealed MAGPy probe placed inside the ELI phantom filled with tissue simulating liquid (TSL) HBBL4-250V3, which has the nominal values of $\epsilon_r = 55$ and $\sigma = 0.75\,\mathrm{S/m}$. The phantom was placed above the 400 kHz reference source (i.e., V-Coil50/400) at d $\approx$ 2 mm. The current fed to the coil was determined by measuring the voltage across the current monitoring resistor with an oscilloscope. A photo of the setup is shown in Figure 12. The probe was moved to different distances (with a DASY robot) along a vertical observation line. The incident H-field was measured at each distance for three cases: (1) without TSL, (2) with TSL of a filling depth of 105 mm, and (3) with TSL of a filling depth of 150 mm. The measurement for the case without TSL was repeated four times. The measurements for the cases with TSL were repeated twice, and were made between the second and third measurements for the case without TSL. The H-field measurement results are illustrated in Figure 13. The deviations are well within the expected measurement repeatability of $<$0.5 dB and confirms the theoretical considerations that the effect is less than 1% or 0.1 dB.

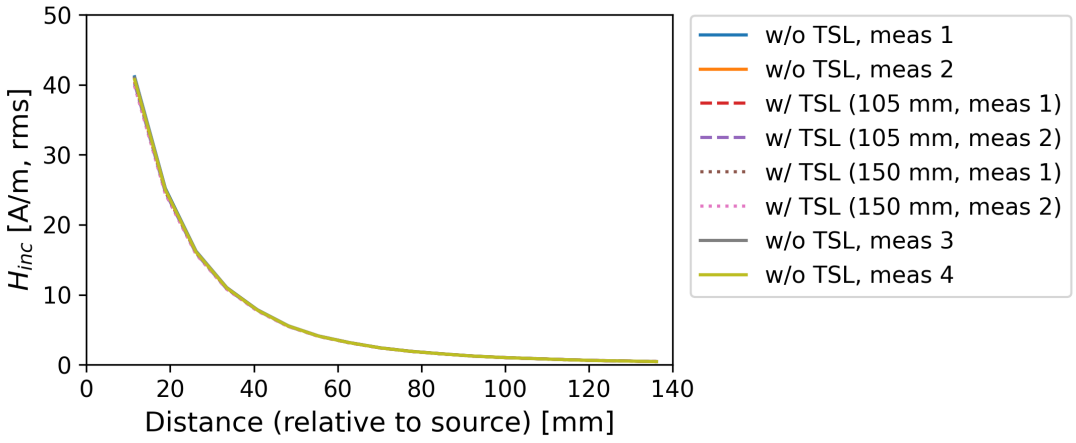

(a) Total H-fields along the vertical line for three TSL-filling cases

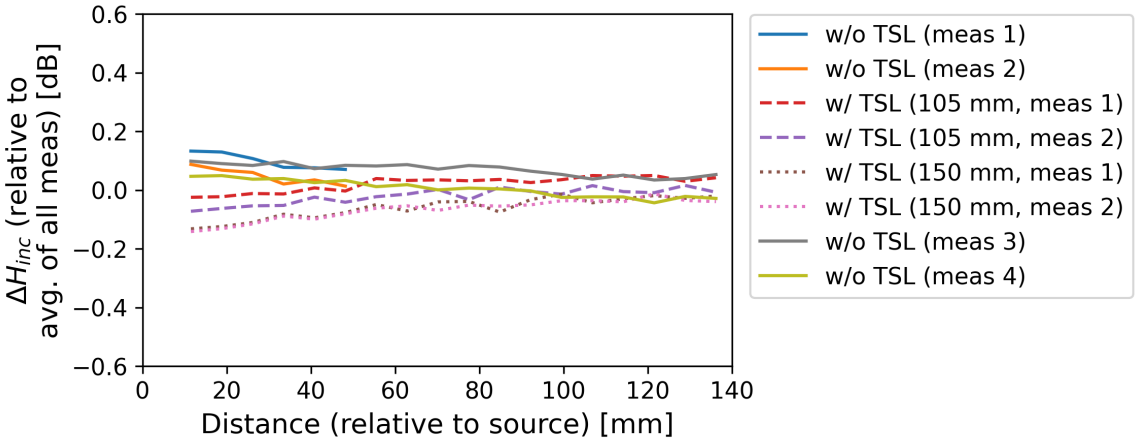

(b) Deviations in the total H-field along the vertical line for three TSL-filling cases

Figure 13: Measurement results of the incident H-field, confirming its insensitivity to the presence of the phantom. The results showed include three cases: with TSL of a filling depth of 105 mm, with TSL of a filling depth of 150 mm, without TSL.

B.5 Conclusions

The effect of the phantom loading or backscattering is less than 1% for frequencies <4 MHz as derived from theoretical considerations, supported by simulations and verified by measurements. Therefore, when the evaluation is performed on the incident field only, i.e., without phantom, the coupling between phantom and source results in an additional uncertainty of 0.1 dB. Neglecting the flux cancellation due to the induced current in the phantom leads to a small overestimation and therefore is conservative and is not considered in the uncertainty estimation.

C Validation of the DASY8/6 Module WPT Evaluation of the Total Field

C.1 Evaluation of the Induced Fields by the Validation Source V-Coil50/6780 V2

C.1.1 Instrumentation and V&V Sources

The configuration of the DASY6 Module WPT system used in the validation measurements is listed in Table 8.

System	Type:	DASY6 Module WPT
	Software Version:	V2.6
	Manufacturer:	Schmid & Partner Engineering AG, Switzerland
Positioner	Robot:	TX90 XL
	Serial No:	F/18/0004593/A/001
	Controller:	CS8C
	Serial No:	F/18/0004593/C/001
	Manufacturer:	Stäubli, France
Probe	Type:	MAGPy-8H3D+E3D V2
	Serial Number:	3065
	Calibrated On:	Apr. 6, 2023
	Next Calibration:	Apr., 2024
	Frequency Range:	3 kHz–10 MHz
	H-Field Dynamic Range:	0.1–3200 A/m
	E-Field Dynamic Range:	0.1–2000 V/m
	H-Field Sensor Area:	1 cm^2
	E-Field Sensor Length:	5 cm
	Probe Length:	335 mm
	Probe Tip Diameter:	60 mm (flat tip)
	Manufacturer:	Schmid & Partner Engineering AG, Switzerland
6.78 MHz Verification Source	Source Model:	V-Coil50/6780 V2
	Source Serial No.:	1014
	Source Dimensions:	250 mm×125 mm×35 mm
	Source Output Freq.:	6.78 MHz
	Source Current:	0.394 A
	Source Evaluated On:	Jan. 29, 2024
	Source Manufacturer:	Schmid & Partner Engineering AG, Switzerland

Table 8: DASY6 Module WPT system and Validation Source

C.1.2 Method

The 6.78 MHz validation source was simulated with the fullwave finite-difference time-domain solver and the magneto quasi-static (MQS) solver in Sim4Life V7.2, and also measured with DASY6 Module WPT V2.6. The total field approximation was also applied, with the incident E-field obtained from simulation/measurement as the input. This approaches a worst-case evaluation, as the contributions of the incident E-field to the induced E-field is further reduced at lower frequencies.

C.1.3 Results

The results are summarized in Table 9.

Simulation vs. Measurement	Method	pE_{ind} [V/m]	$psSAR_{1g}$ [W/kg]	$psSAR_{10g}$ [W/kg]
Simulation	Fullwave	109	4.05	1.97
	MQS	107	4.06	1.95
	Total field approximation	107	4.06	1.95
Measurement	MQS	104	3.97	1.97
	Total field approximation	104	3.97	1.97

Table 9: Results of the induced E-field evaluations performed with Sim4Life V7.2 and DASY6 Module WPT V2.6.

C.2 Conclusions

The MQS assessment implemented provides accurate results for the E-field and SAR induced by the H-field only. The total field approximation implemented in DASY8/6 Module WPT V2.6+ provides a reliable assessment of the maximum induced fields, e.g., psSAR1g/10g and pE_{ind}.

D Verification Report of the Low Frequency Magneto Quasi-Static Solver

THESSALONIKI SOFTWARE SOLUTIONS

Verification Report MQS001AA201507

Sim4Life and SEMCAD X Low Frequency Magneto Quasi−Static Solver

George Tsanidis[1], Theodoros Samaras[2]

Thessaloniki, July 2015

[1]**THESS S.A., Technopolis ICT Business Park, 57001 Thessaloniki, Greece**
[2]**Department of Physics, Aristotle University of Thessaloniki, 54124 Thessaloniki, Greece**

Confidentiality Note All information contained in this document including commercial and technical information, description of processes graphics, figures, tables, drawings, etc. is strictly confidential and for recipients internal use only. Recipient shall not in any manner disclose any of the information contained in this document to any third party without prior written consent of ZMT Zurich MedTech AG (ZMT) except where it is required for the submission to governmental approval bodies.

Executive Summary

The THESS S.A. was mandated by ZMT Zurich MedTech AG (Offer No. 1420) to independently verify the Sim4Life and SEMCAD X platforms. The here documented MQS001AA201507 verification benchmark for the EM LF Magneto Quasi-static Solver was developed and tested for the Sim4Life Version v2.0 and SEMCAD X v14.8, and documented such that ZMT can automatically run the test for any new software version.

The MQS001AA201504 benchmark verifies the EM LF Magneto Quasi-static Solver against the analytically calculated value of the magnetic field generated by a circular thin-wire coil inside an adjacent conducting sphere. This benchmark tests the following solver features:

- that the EM LF Magneto Quasi-static Solver converges to the right solution
- that material interfaces are properly handled
- that the Biot-Savart sources are correctly implemented
- that post-processing correctly calculates derived quantities such as current density.

The agreement of the theoretically calculated magnetic field with the values derived from the Sim4Life and SEMCAD X platform is very good: The current density values at different positions inside the sphere match for the two methods with a deviation smaller than 0.5% for the finer discretization of the computational domain. With increasing grid resolution, the simulation results converge to the analytical solution.

In conclusion, the numerical MQS solver of Sim4Life and SEMCAD X therefore meets the requirements for modeling the magneto-quasistatic equation.

Contents

1 Objectives

The objective of this verification report MQS001AA201507 is to document the verification of the Sim4Life v2.0 and SEMCAD X v14.8 Low Frequency Magneto Quasi-static Solver by comparing numerical to analytical solutions of a specific problem.

The MQS solver first calculates a magneto-static vector potential (A_0) using the Biot-Savart law and subsequently determines the induced E-fields and currents using potential continuity while considering the inhomogeneous dielectric property distributions in the human anatomy [2]. The equation $\nabla \cdot \sigma \nabla \phi = -j\omega \nabla \cdot (\sigma A_0)$ is solved (σ: conductivity, ω: angular frequency, ϕ: electric scalar potential) which is valid at frequencies where ohmic currents dominate over displacement currents.

The following features of the EM LF Magneto Quasi-static solver have been identified as fundamental and requiring verification:

- that the EM LF Magneto Quasi-static Solver converges to the right solution
- that material interfaces are properly handled
- that the Biot-Savart sources are correctly implemented
- that post-processing correctly calculates derived quantities such as current density

For that purpose an analytically solvable benchmark case has been chosen such that it makes use and covers all of these critical features. The benchmark is a homogeneous sphere exposed to current carrying ring wire.

2 Methodology

2.1 Introduction

The field of Magnetostatics was widely studied during the 19th century. The work of J.B. Biot and F. Savart made possible the calculation of the magnetic field originating from an electric current. They provide an approximation of the Maxwell equations valid for low frequency, provided a quasi-static behavior that can be assumed in the case of slow time variations (low frequency) and sufficiently small dimensions. The approximation condition is $\left(\frac{d}{\lambda}\right)^2 << 1$, where d is the diameter of the computational domain and λ the wavelength. The law of Biot-Savart can be used in order to easily calculate the value of the magnetic field inside a head-sized sphere, with the dielectric properties of the human brain, created by an adjacent circular loop coil.

The numerically derived results of the EM LF Magneto Quasi-static Solver of the Sim4Life and SEMCAD X platform are compared with the theoretically calculated results in order to evaluate the reliability and accuracy of the former and this deviation is examined with respect to

- the relative solver tolerance used to terminate the numerical process,
- the grid step of the computational domain,
- the implementation of the material interfaces

2.2 Analytical solution

A surface coil (loop of uniform current) adjacent to a homogeneous conducting sphere can be used in order to predict the performance of MRI surface coils close to the human head. By solving the inhomogeneous boundary value problem of the system, the electromagnetic field inside the sphere can be calculated. The sphere's parameters, i.e. the relative dielectric constant ϵ_r and the conductivity σ, are chosen so as to model the human brain.

The magnetic field produced by the surface coil adjacent to the homogeneous sphere has been calculated by solving the inhomogeneous boundary value problem of a ring of radius R carrying uniform current I adjacent to a conducting dielectric sphere of radius α centered at the origin of a spherical coordinate system (Fig. 1).

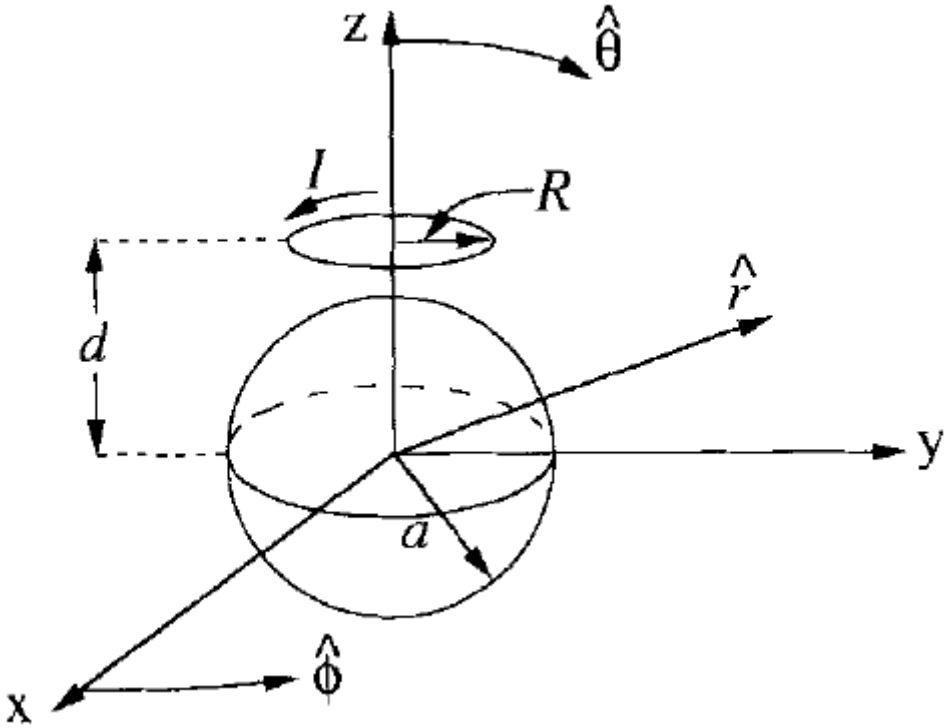

Figure 1: Schematic arrangement of a homogeneous conductive sphere near a circular current loop. The sphere is centered at the origin of the spherical coordinate system

The magnetic field inside the sphere is given by [1]

$$B_r(r,\theta,\phi) = \sum_{i=1}^{\infty} b_{l0}\sqrt{\frac{l(l+1)(2l+1)}{4\pi}}P_i(cos\theta)\frac{j_i(k^{in}r)}{k^{in}r} \tag{1}$$

$$B_\theta(r,\theta,\phi) = -\sum_{i=1}^{\infty} b_{l0}\sqrt{\frac{(2l+1)}{l(l+1)4\pi}}sin\theta\frac{dP_i(cos\theta)}{dcos\theta}\frac{1}{k^{in}r}\frac{\vartheta(j_i(k^{in}r))}{\vartheta r} \tag{2}$$

$$B_\phi(r,\theta,\phi) = 0 \tag{3}$$

where $j_i(kr)$ denotes the spherical Bessel functions of the first kind and $P_i(cos\theta)$ are Legendre polynomials.

The wavenumber inside the sphere k^{in} is obtained from Maxwell's equation ,

$$\nabla \times \vec{B} = \mu_0\vec{J} + \mu_0\epsilon\frac{\partial\vec{E}}{\partial t}. \tag{4}$$

where μ_0 is the permeability of free space. Substituting $\vec{J} = \sigma\vec{E}$ and defining the relative dielectric constant as $\epsilon_r = \frac{\epsilon}{\epsilon_0}$ equation (4) is transformed to

$$i\omega\nabla \times \vec{B} = (i\omega\mu_0\sigma + \epsilon_r\frac{\omega^2}{c^2})\vec{E} \tag{5}$$

where ω is angular frequency, σ is electrical conductivity and c is the speed of light. The wave number inside the sphere k^{in} is the square root of the coefficient of

$$(k^{in})^2 = i\omega\mu_0\sigma + \epsilon_r\frac{\omega^2}{c^2} \tag{6}$$

Solving equation (5) for the electric field, one is allowed to express the current density $\vec{J}$ as

$$J_\phi(r,\theta,\phi) = \frac{i\omega\sigma}{k^{in}} \sum_{i=1}^{\infty} b_{l0} \sqrt{\frac{(2l+1)}{l(l+1)4\pi}} j_i(k^{in}r) sin\theta \frac{dP_i(cos\theta)}{dcos\theta} \tag{7}$$

The b_{l0} are found by satisfying the boundary conditions of the magnetic field at the surface of a homogeneous conducting, dielectric sphere given an incident magnetic field produced by an adjacent ring of uniform current

$$\begin{aligned} b_{l0} = \mu_0 I 2\pi \sqrt{\frac{(2l+1)}{l(l+1)4\pi}} \frac{(k^{out})^2 R^2 {h_i}^{(1)}(k^{out}\sqrt{d^2+R^2})}{\sqrt{d^2+b^2}} \frac{dP_i(\xi)}{d\xi} \\ \frac{k^{in}(j_i(k^{out}\alpha)y_{i+1}(k^{out}\alpha) - y_i(k^{out}\alpha)j_{i+1}(k^{out}\alpha))}{k^{in}{h_i}^{(1)}(k^{out}\alpha)j_{i+1}(k^{in}\alpha) - k^{out}j_i(k^{in}\alpha){h_{i+1}}^{(1)}(k^{out}\alpha)} \end{aligned} \tag{8}$$

where k^{out} is the wave number in free space, y_i and ${h_i}^{(1)}$ are spherical Bessel functions of the second and third kinds, respectively, and ξ is the cosine of the angle subtended by the loop $\xi = \frac{d}{\sqrt{d^2+R^2}}$

2.3 Numerical Modeling

This verification study intends to compare the current density J calculated by the analytical solution, with the numerical results obtained by Sim4Life and SEMCAD X for the same problem. A sphere of 60mm radius and a surface coil of 20mm radius were placed at a distance of 50mm between the coil center and the nearest point of the sphere. For mathematical convenience the z axis of the coordinate system was chosen to be parallel to the axis of the coil. The sphere's relative dielectric permittivity ϵ_r and electrical conductivity σ are that of a human brain (white matter: $\sigma = 0.0626\, S/m$, $\epsilon_r = 69800$).

3 Results

3.1 Criterion of convergence

No difference in the numerical results was observed when changing the value of relative tolerance (which is the criterion of convergence for the computational process) from 10^{-6} to 10^{-12}. In particular the maximum difference between the values of the electric field induced inside the sphere, as extracted at the center, is 0.000172%.

3.2 Grid step

Simulations with uniform grids and varying grid step were performed (0.3, 0.5, 1, 2, 3, 4 and 5 mm) and they gave similar results (Fig. 2). For comparison the magnetic field along two axes (Fig. 3) was extracted and is presented with the theoretical, as is calculated by the Law of Biot-Savart (Fig. 4) and (Fig. 5).

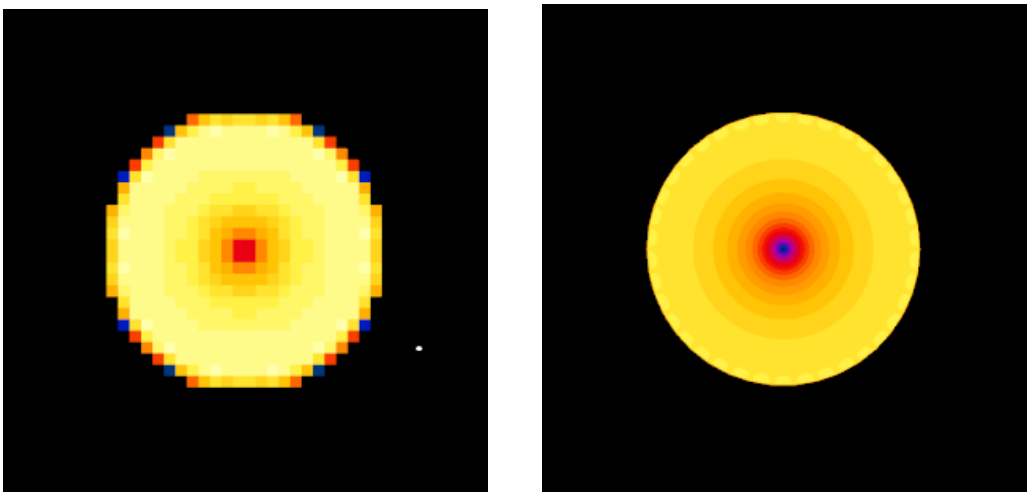

Figure 2: Slice views of the electric field inside the sphere for coarse (Grid Step: 5mm) and fine grid (Grid Step: 0.3mm).

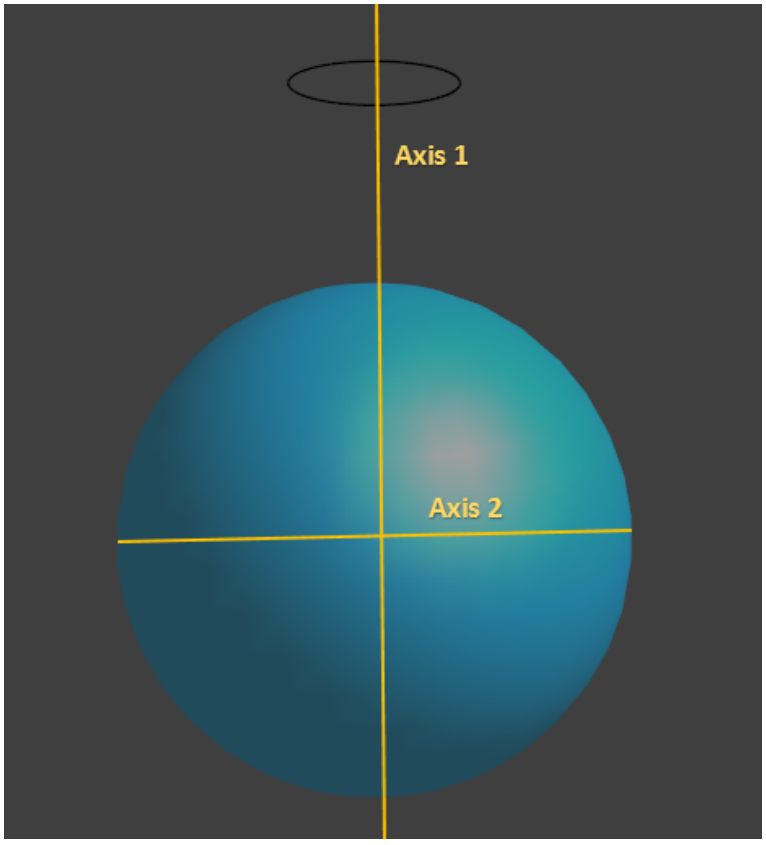

Figure 3: The two axes of extraction.

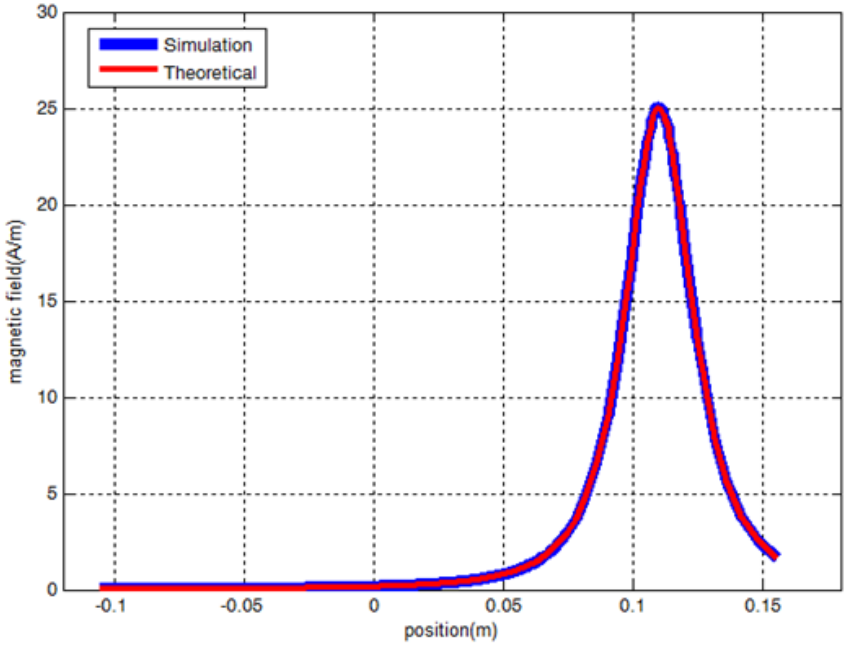

Figure 4: The extracted and the theoretical magnetic field along Axis 1 (Grid step: 0.3mm)

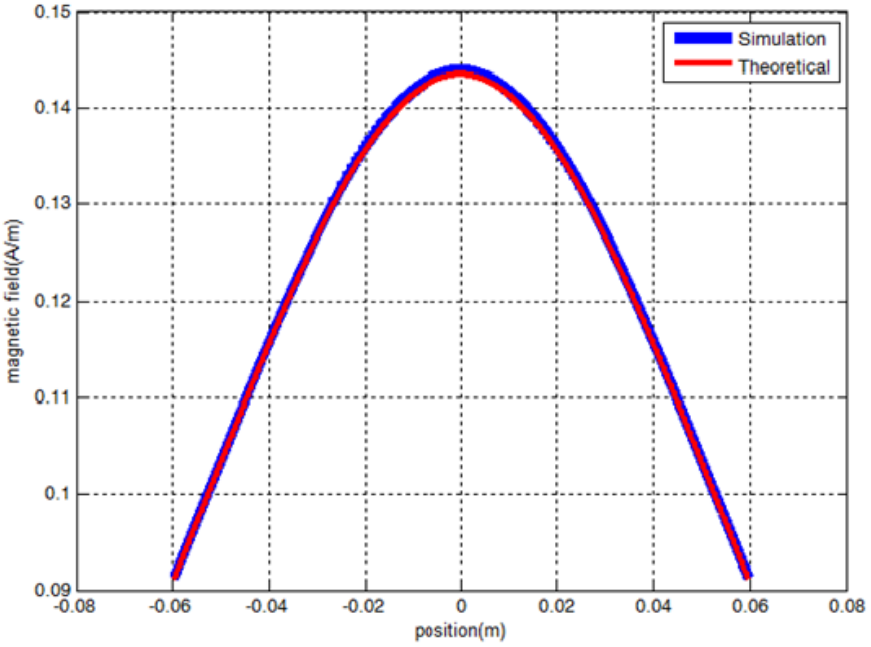

Figure 5: The extracted and the theoretical magnetic field along Axis 2 (Grid step: 0.3mm)

For the comparison between the theoretical and the simulated current distribution at the sphere, the deviation of the numerical solution from the analytical solution was evaluated at circles of distances 5, 10, 30 and 50mm from the center of the sphere(Fig. 6).

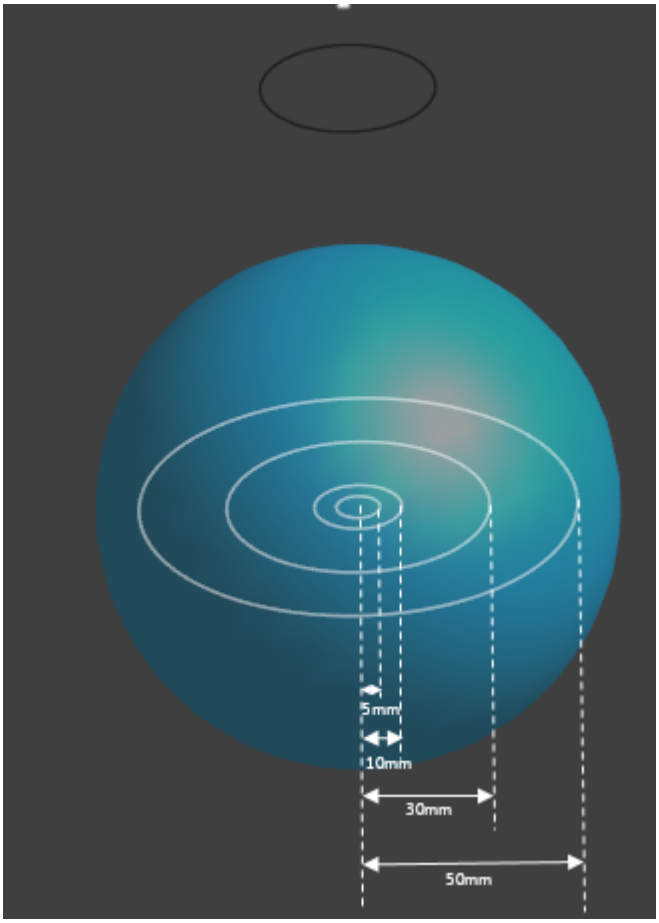

]

Figure 6: The two axes of extraction.

The computational space was discretized with a uniform grid of variable maximum step and the deviation between the numerical (N) and the analytical (T) solution for the current density was evaluated at the points of the numerical solution:

$$deviation\, U = |\frac{N-T}{T}|100\% \tag{9}$$

The maximum deviation on the above circles are shown in (Fig. 7). It is clear that, in every case, for a finer discretization of the grid (smaller grid step) the deviation continuously decreases and the numerical solution converges to the analytical solution.

3.3 Material interfaces

For the model with uniform grid step of 0.1mm, the radial component of the magnetic field was extracted on either side of the surface of the sphere, along a circle. At material interfaces, i.e., at the interface of air with the sphere, the radial component of the magnetic field should be identical when approaching the interface from both sides. The absolute value of the relative difference between the two values is shown in (Fig. 8). The deviation never exceeds 0.14% indicating that material interfaces are correctly handled by the solver.

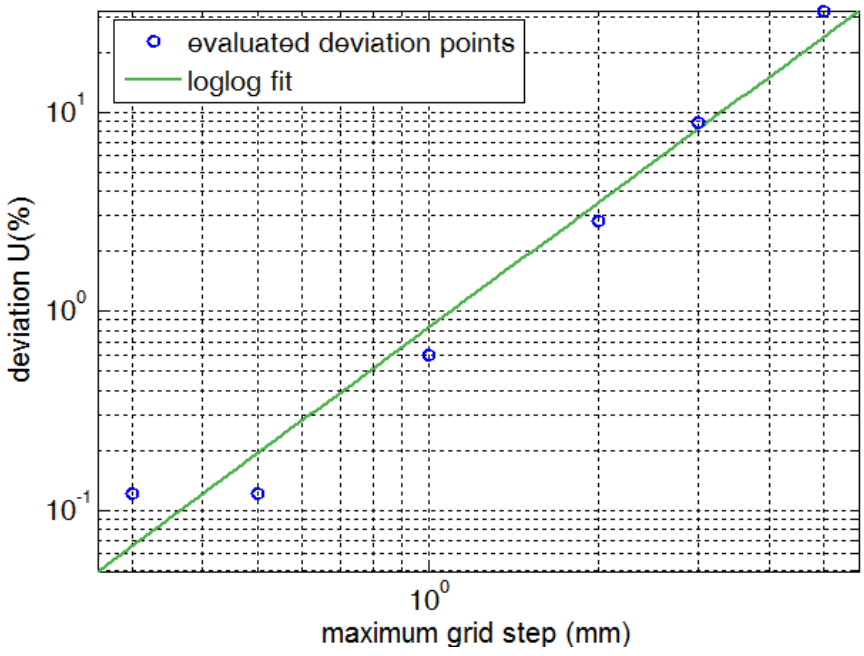
evaluated deviation points
loglog fit
deviation U(%)
10^1
10^0
10^{-1}
10^0
maximum grid step (mm)

]

(a)

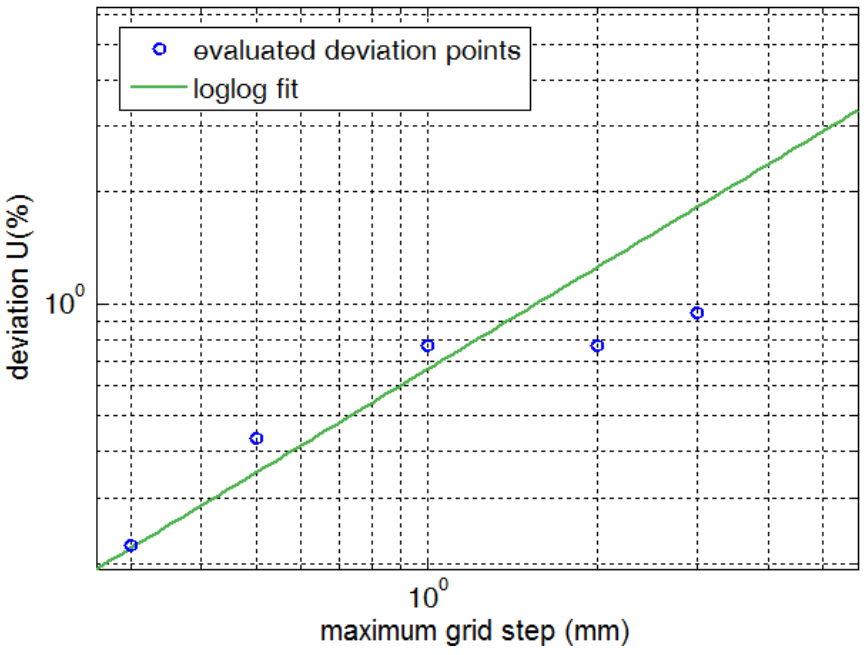
evaluated deviation points
loglog fit
deviation U(%)
10^0
10^0
maximum grid step (mm)

(b)

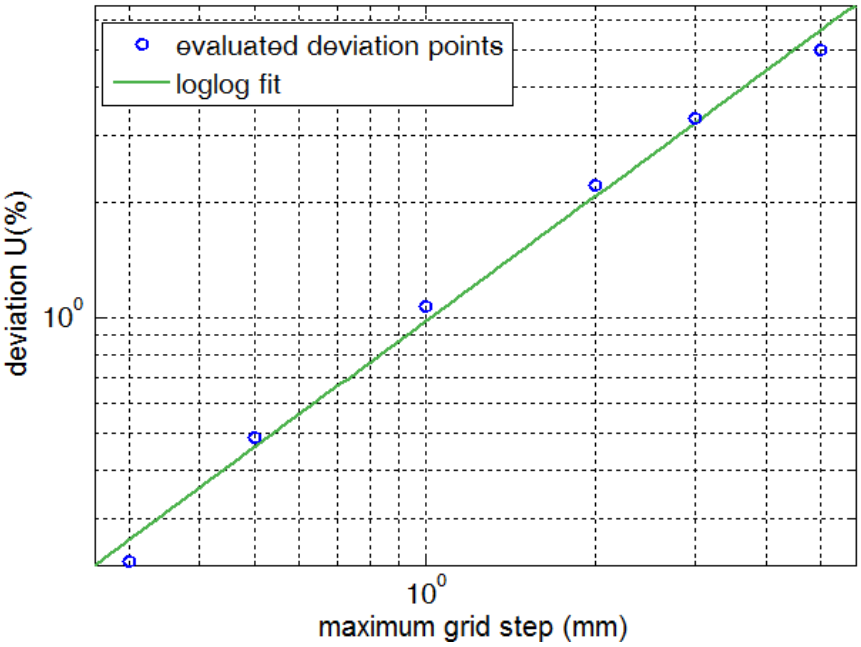

]

(a)

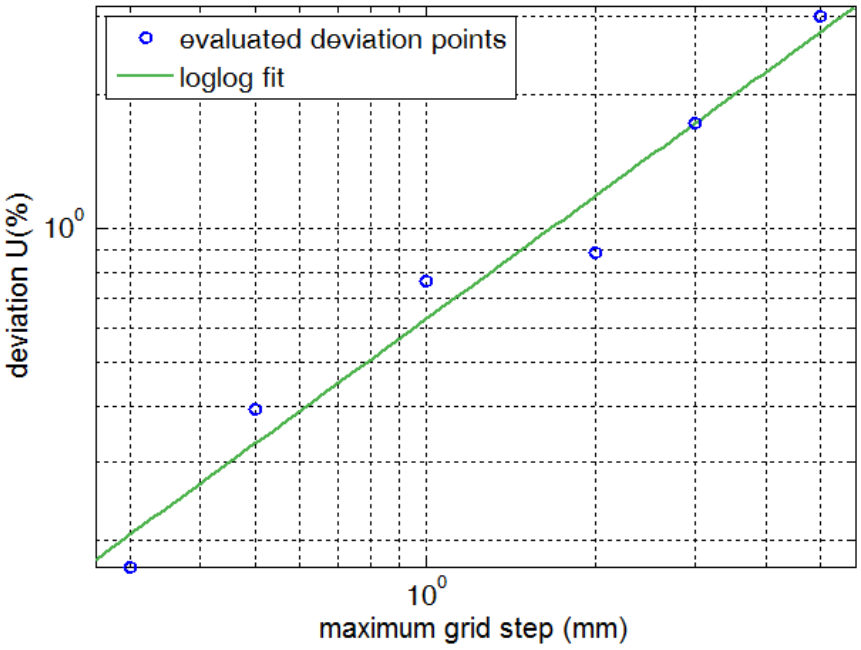

(b)

Figure 7: Maximum deviation (see equation (9)) of the numerical from the analytical solution along a circle at distance of 5mm (a), 10mm (b) 30mm (c) and 50mm (d) from the center of the sphere as a function of the maximum grid step.

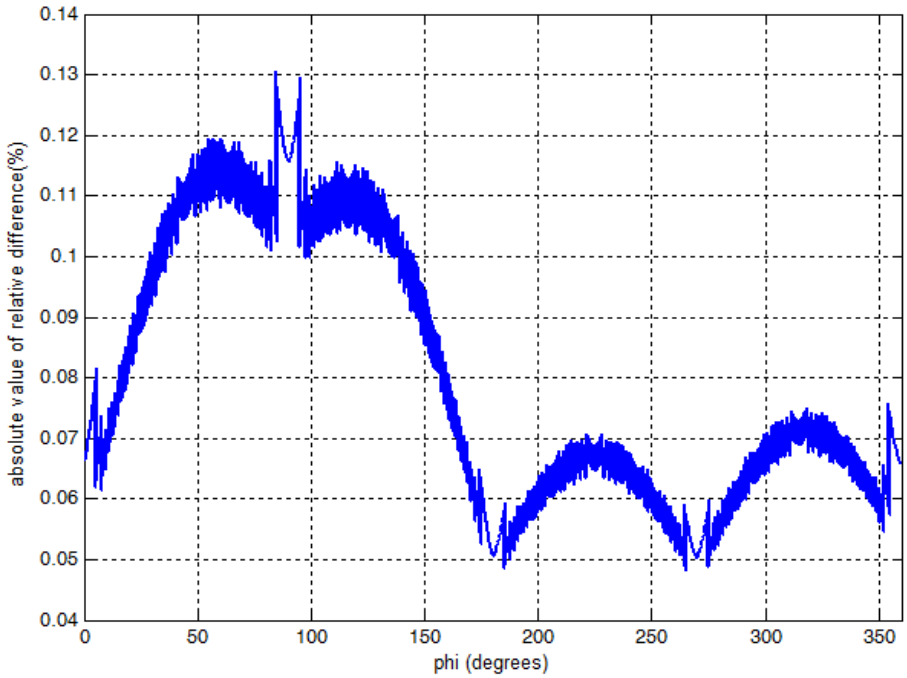

]

Figure 8: Relative difference (absolute value) between the perpendicular magnetic field components on either side of the sphere's surface. (Grid step: 0.1mm).

4 Conclusion

The purpose of this verification study was to examine the agreement between the numerical results obtained by the Sim4Life and SEMCAD X LF MagnetoQuasi-static solver and the analytically obtained results. It was shown that grid resolution has an important impact on accuracy. It is possible to keep the deviation between numerical and analytical solutions lower than 0.5%, by choosing the appropriate discretization (grid step). With increasing resolution, the simulation results converge to the analytical solution. Proper numerical convergence has been ascertained by varying the convergence criterium. The benchmark case tests the following fundamental solver features:

- that the EM LF Magneto Quasi-static Solver converges to the right solution
- that material interfaces are properly handled
- that the Biot-Savart sources are correctly implemented
- that post-processing correctly calculates derived quantities such as current density

The current density values at different positions inside the sphere match for the two methods with a deviation smaller than 0.5% for the finer discretization of the computational domain. With increasing resolution, the simulation results converge to the analytical solution.

Neither the spatial discretization nor the solution algorithm employed by Sim4Life and SEMCAD X use any assumptions based on the shape of the computational domain. This renders the approach suitable for any complex structures which might occur in biomedical applications. Because of this generalized verification approach it is valid to expect similarly accurate performance of the solver in simple geometries like the presented benchmarks and in more complex geometrical models.

In conclusion, the numerical MQS solver of Sim4Life and SEMCAD X therefore meets the requirements for modeling the magneto-quasistatic equation.

References

[1] J.R. Keltner. *Electromagnetic Fields of Surface Coil in Vivo NMR at High Frequencies, p.467-480, Magnetic Resonance in Medicine 22,* 1990.

[2] ZMT. *Sim4Life User Manual*, ZMT Zurich Med Tech, Zurich, Switzerland, 2015.

E Procedure to Test Two-Coil WPT Systems

The test procedure to test WPT systems with two coils working at different fundamental frequencies is outlined here.

- set the peak frequency search range to only capture the fundamental frequency of the first coil
- perform a volume scan and determine the induced fields due to the first coil according to the procedure described in Section 5.2
- set the peak frequency search range to only capture the fundamental frequency of the second coil
- perform a volume scan and determine the induced fields due to the second coil according to the procedure described in Section 5.2
- combine the exposure ratios for the induced fields due to the two coils